The Scaling of Signal-to-Noise in Heat-Assisted Magnetic Recording

Jian-Gang Zhu, *Fellow, IEEE*

Data Storage Systems Center, Department of Electrical and Computer Engineering, Carnegie Mellon University, Pittsburgh, PA 15213 USA

This article presents a systematic micromagnetic modeling study on recording characteristics in heat-assisted magnetic recording (HAMR). Utilizing a novel micromagnetic model developed based on the $L1_0$ ordering atomic structure of the FePt grains, the study shows that the medium noise caused by grain-to-grain Curie temperature variations can be effectively suppressed with sufficiently high thermal recording gradient along with sufficient head field amplitude. The rest of the article focuses on the thermal noise and its correlations with various recording parameters.

***Index Terms*— ADC, curie temperature, FePt, hard disk drive (HDD), heat-assisted magnetic recording (HAMR), $L1_0$, SNR, thermal gradient (TG), transition jitter noise.**

I. Introduction

HEAT-ASSISTED magnetic recording (HAMR) brings exciting promises for the future of hard disk drive (HDD) recording technology [1], [2], [3], [4], [5], [6]. Just like all innovations, HAMR also brings many new technological challenges, some of which have become the driving force for studies that advance our understanding of new recording physics and directly provide possible solutions. In particular, micromagnetic modeling work carried out over the past 15 years has unveiled some of the important insights on HAMR recording processes [7], [8], [9], [10], [11], [12], [13], [14], [15], [16], [17], [18], [19], [20], [21], [22], [23], [24].

It has been well recognized that thermal gradient (TG) in recording is critically important to suppress medium noise [25]. However, in practice, the bit error rate (BER) benefit seems to saturate at relatively low TG [25], [26], limiting the expected areal density gain for the recording. In searching for the answer to this puzzle, systematic micromagnetic modeling and simulation work is conducted and presented here. The study focuses on the understanding of the correlation between TG and grain-to-grain Curie temperature variation. At the same time, I will try to establish correlations between the thermal noise and other recording parameters, such as head field amplitude and disk speed during writing.

II. Model and Simulations

The micromagnetic model employed here has been developed to incorporate the physical nature of the distinctive atomic structure in $L1_0$ FePt grains of the recording media [21]. In a perfectly ordered $L1_0$ FePt single crystal grain, monolayers of pure Fe and pure Pt alternate in the ordering direction [27], [28]. Because of this ordered atomic structure, near but below Curie temperature, the ferromagnetic exchange coupling within each Fe monolayers would dominate whereas the exchange coupling between adjacent Fe monolayers, mediated by the spin-polarized Pt monolayer in between, is relatively weaker [29]. Considering this important fact, each FePt grain in the HAMR granular media studied here is modeled by a stack of 30 macro-spins [21] with each macro-spin representing the magnetization of a single Fe atomic monolayer, as illustrated in Fig. 1. This approach effectively assumes that each Fe monolayer is always uniformly magnetized. The 30 Fe monolayer stack corresponds to a single $L1_0$ FePt grain of a height 11.52 nm, using the lattice spacing of $c = 0.384$ nm in the ordering direction [28]. While the magnetic moment of Pt monolayers is ignored in this model, the Pt-mediated exchange coupling between adjacent Fe monolayers is incorporated. Each macro-spin is assumed to follow the temperature dependence of the magnetization:

$$M(T) = M(0)\left(1 - \frac{T}{T_C}\right)^{\frac{1}{3}} \tag{1}$$

and anisotropy field [26]

$$H_k(T) = H_k(0)\left(1 - \frac{T}{T_C}\right)^{\frac{1.1}{3}} \tag{2}$$

with easy axis oriented along the ordering direction, which is perpendicular to the film plane for this article.

The model, thus, enables the modeling of nonuniform temperature as well as different T_c through the depth of a grain. However, in this study, the Curie temperature T_c is assumed to be the same for all the monolayers within the grain while T_c can vary from grain to grain according to a Gaussian distribution. As shown in Fig. 1, a practical HAMR media is represented by a Voronoi assembly of the modeled $L1_0$ FePt grains. For all the cases presented in this article, the mean T_c is assumed to be 675 K. The created grain assembly has a 15% grain size distribution with mean grain diameter at $D = 7$ nm. No correlation between the grain Curie temperature and the grain size is assumed. The anisotropy field of every

Manuscript received 4 August 2023; revised 29 August 2023; accepted 6 September 2023. Date of publication 22 September 2023; date of current version 25 April 2024. Corresponding author: J.-G. Zhu (e-mail: jzhu@cmu.edu).

Color versions of one or more figures in this article are available at https://doi.org/10.1109/TMAG.2023.3315285.

Digital Object Identifier 10.1109/TMAG.2023.3315285

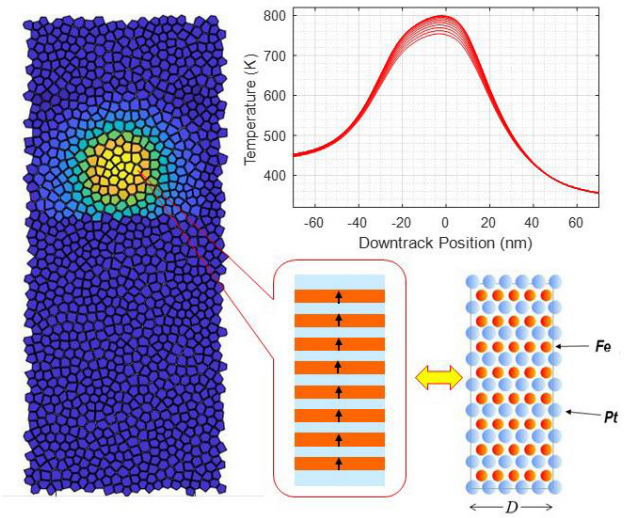

Fig. 1. Left: Modeled FePt granular media with temperature profile during a recording. Top Right: Recording thermal profile calculated using COMSOL from top to bottom at different depth of medium grain. Bottom Right: Illustration of each grain is modeled by a stack of macro-spins with each macro-spin modeling a single Fe atomic monolayer. Adjacent Fe monolayers are coupled by the ferromagnetic exchange interaction mediated by the Pt monolyaer in between.

grain is set to be the same with $H_k(\mathrm{RT}) = 8$ Tesla at room temperature without any variation from grain to grain.

Three-dimensional recording temperature profiles, with one shown in Fig. 1, are calculated using COMSOL software. The peak temperature is 800 K for all the cases in this article. In mapping the thermal profile to the actual grains in the medium at any moment, the average temperature over the lateral area of a grain is used. The dynamic orientation of each macro-spin follows the Landau-Lifshitz–Gilbert gyromagnetic equation of motion:

$$\frac{d\vec{m}}{dt} = \frac{\gamma}{1+\alpha^2}\vec{m}\times\vec{H} - \frac{\alpha\gamma}{1+\alpha^2}\vec{m}\times\vec{m}\times\vec{H} \tag{3}$$

where $\vec{m}$ is the unit vector of the magnetic moment for the macro-spin, γ is the gyromagnetic ratio, α is the Gilbert damping constant, and $\vec{H}$ is the effective field on the macro-spin, which includes

$$\vec{H} = \vec{H}_{\mathrm{an}} + \vec{H}_{\mathrm{ex}} + \vec{H}_{\mathrm{mag}} + \vec{H}_{\mathrm{head}} + \vec{H}_{\mathrm{thermal}} \tag{4}$$

where the right-hand side are magnetic anisotropy field, the exchange coupling field between adjacent Fe monolayers within a grain, magnetostatic fields, head field, and thermal magnetic Langevin field, respectively. In particular, the inter-layer exchange field is

$$\vec{H}_{\mathrm{ex}} = \frac{2A^*}{c^2}(\vec{m}_{i+1} + \vec{m}_{i-1}) \tag{5}$$

where $\vec{m}_{i+1}$ and $\vec{m}_{i-1}$ are the unit vector of the macro-spins for the adjacent Fe monolayer above and below, respectively, c is the distance between adjacent Fe monolayers, and A^* is the effective exchange stiffness constant between the adjacent Fe monolayers within a gran. Since this exchange coupling is mediated by the spin-polarized Pt atoms in between, it is reasonable to assume that the exchange coupling would also

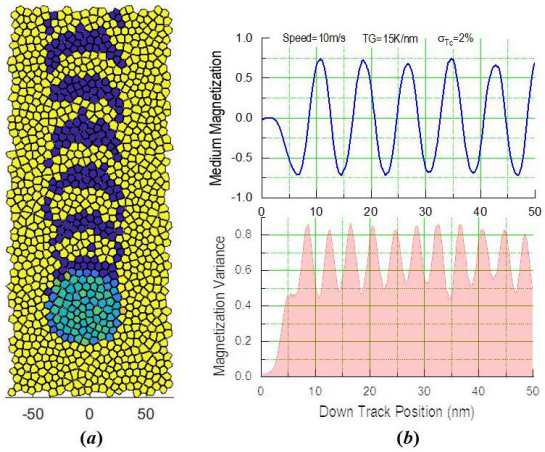

Fig. 2. (a) Simulated recording process with color representing the perpendicular component of magnetization of each grain. Zero magnetization for the region above Curie temperature shown in green. Yellow and blue show opposition magnetization components. (b) Mean readback" magnetization (upper) and corresponding variance (lower) for a read width of 30 nm.

be proportional to the magnetization level of the two adjacent Fe monolayers

$$A^* = A_0^*\left(1 - \frac{T}{T_C}\right)^{\frac{1}{3}}. \tag{6}$$

This is because the Pt spin polarization should be proportional to the magnetic moment of Fe monolayers. For all the calculation results presented here, $A_0^* = 0.45 \times 10^{-6}$ erg/cm is used and the reason for choosing this particular value will be discussed later in the article. The head field is assumed to be spatially uniform and its direction is assumed to be tilted toward the down track direction at an angle of 20° with respect to the perpendicular direction. The thermal Langevin magnetic field is used to model the thermal effect which has been described in detail in [7], [31], [32], and [33]. For all the calculations presented here, a Gilbert damping constant $\alpha = 0.2$ is used which gives reasonable match between experimental measurements and modeling results. Existing theoretical and experimental investigations have indicated significant rise of the Gilbert damping constant near Curie temperature [34], [35], [36].

Fig. 2 shows simulated recording process (left) with color spectrum representing the perpendicular component of the grain magnetization as yellow for RT $M_s \uparrow$ and deep blue for RT $M_s \downarrow$. The thermal heating spot moves from up to down in a constant speed relative to the granular medium while recording head field reverses its direction over time. Over a rectangular area of 30 nm width (crosstrack) and 2 nm length (downtrack resolution) is performed over a simulated written track (~320 nm in length). For each calculation case, 60 tracks, each with different granular pattern, are simulated. Mean magnetization profile and corresponding variances are calculated. The signal power

$$\mathrm{SP} = \frac{1}{2B}\int_0^{2B} \bar{M}^2 \mathrm{dx} \tag{7}$$

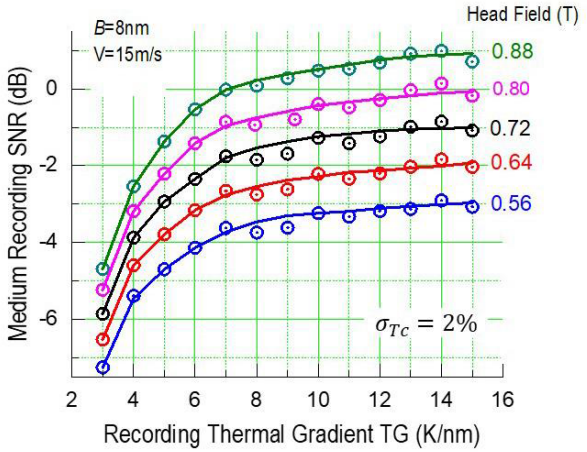

Fig. 3. Calculated SNR as a function of recording TG for a range of head field amplitudes. A standard deviation of $\sigma_{TC} = 2\%$ is assumed for grain Curie temperature distribution. The symbols are actual calculation results and the curves are drawn to guide the eye (for this plot and the rest of the plots in the paper).

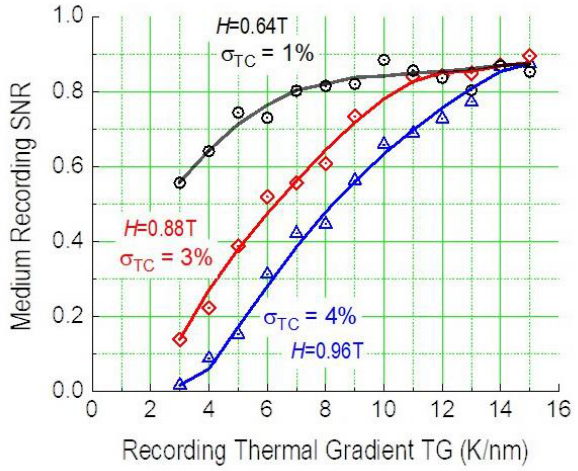

Fig. 4. Calculated SNR for three media of different values of σ_{Tc}. Note for each medium case, head field amplitude is adjusted such that the SNR saturation values at high TG for each case match each other. The results here show with sufficient high TG and raised head field amplitude, the noise arising from grain-go-grain Curie temperature variation can be completely suppressed.

where B is the bit length, and noise power

$$\mathrm{NP} = \frac{1}{2B}\int_0^{2B} \overline{(M-\bar{M})^2}\mathrm{dx}. \tag{8}$$

The signal-to-noise ratio (SNR) is defined as

$$\mathrm{SNR} = \frac{\mathrm{SP}}{\mathrm{NP}}. \tag{9}$$

III. Results and Discussion

Fig. 3 shows calculated SNR as a function of recording TG for a range of head field amplitudes. A standard deviation of $\sigma_{TC} = 2\%$ is assumed for grain Curie temperature distribution. At each field amplitude, SNR rises rapidly with the initial increase of TG followed by slowing down of the increase. The SNR saturation begins around TG = 7 K/nm. The TG dependence is essentially the same for all the cases with different field amplitudes, however, the exact SNR level increases with increasing head field amplitude for the field amplitude range shown in the figure.

The dependence of SNR on recording TG shown in Fig. 3 has been widely observed in practice [25], [26]. The agreement with the experimental measurements not only provides certain degree of validation for the modeling excise presented here, but also enables us to examine the saturation effect. To understand the SNR saturation at relatively high recording TGs, recording simulations on media with different values of σ_{TC} are performed. Fig. 4 shows the calculated SNR as a function of recording TG for three media of different σ_{Tc} values: $\sigma_{Tc} = 1\%$, $\sigma_{Tc} = 3\%$, and $\sigma_{Tc} = 4\%$. For the three corresponding SNR calculations, the head field amplitude is adjusted such that they have the same SNR value at TG = 15 K/nm. The head field values are $H_{\mathrm{head}} = 0.64$ (Tesla), 0.88, and 0.96 for the three cases, respectively. First, we see that the three media with different σ_{Tc} values can reach the same SNR level with sufficient high TG and head field amplitudes. In other words, the SNR degradation caused by grain-to-grain

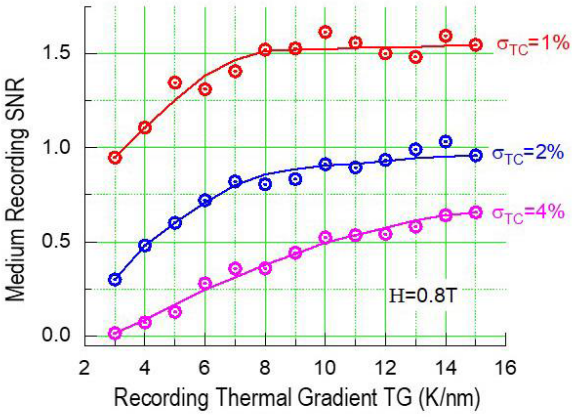

Fig. 5. Calculated SNR as a function of recording TG for three media of different sTc values at the same recording head field amplitude, $H_{\mathrm{head}} = 0.8$ Tesla. The bit length is $B = 15$ nm.

T_C distribution can be completely recovered if recording TG and head field amplitude are sufficient. The broader the Curie temperature distribution, the higher the TG is required along with higher head field amplitude. Conversely, the measurement of the TG at onset of SNR saturation can help to determine the σ_{Tc} value of a medium.

Fig. 5 shows the SNR versus recording TG for the three media at the same field amplitude. Without raise the field amplitude, increase TG alone will not recover the SNR degradation due to grain Tc distribution. Raising field amplitude is equally important to eliminate the SNR impact of grain-to-grain Curie temperature variations.

Sufficiently high head field amplitude, especially when recording TG is high, is important for achieving optimum recording performance. Fig. 6 shows three simulated recording tracks for three different field amplitudes. The recorded bit patterns at the lower field amplitudes appear to be incomplete: some of the grains magnetized in the wrong direction. The situation evidently improves with the higher field amplitudes

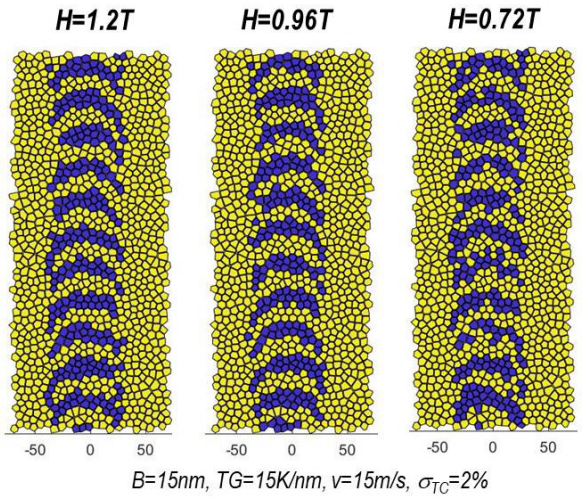

Fig. 6. Simulated recording tracks at three different head field amplitude. The TG is TG = 15 K/nm. Comparing the recorded magnetization patterns between different head field amplitudes, one can see that the recording patterns are incomplete with grains magnetized in wrong directions. Repeating the exact same recording process with the same granular grain structure, the wrongly magnetized grains are different every time since it is caused by the random process, a nature of thermal noise in heat-assisted recording.

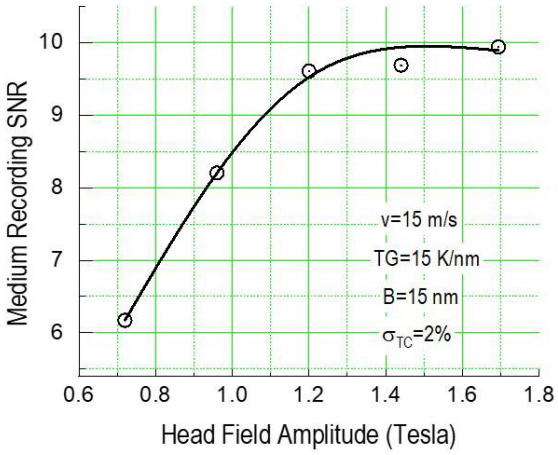

Fig. 7. Calculated recording SNR as function of head field amplitude. The recording TG is TG = 15 K/nm. The linear density is $D = 1700$ KFCI, corresponding to a bit length $B = 15$ nm.

as the percentage of wrongly magnetized grains becomes less. Fig. 7 shows the calculated SNR as a function of head field amplitude. For the calculated results, the recording TG is set at TG = 15 K/nm. As shown in the figure, initial increase of head field amplitudes yields significant increase of the recording SNR. As the head field approaches $H_{\text{head}} = 1.2$ Tesla, SNR starts to level off, continue to increase head field amplitude, the SNR starts to decrease because erasure-after-write starts to become more significant [7].

In HAMR, magnetic bits, or transitions, are formed at temperatures only slightly below the Curie temperature, which is significantly higher than the ambient. At such recording temperatures, the grain magnetization level is significantly below that of the room temperature. The ratio of the magnetic potential energy (due to the recording head field) and thermal

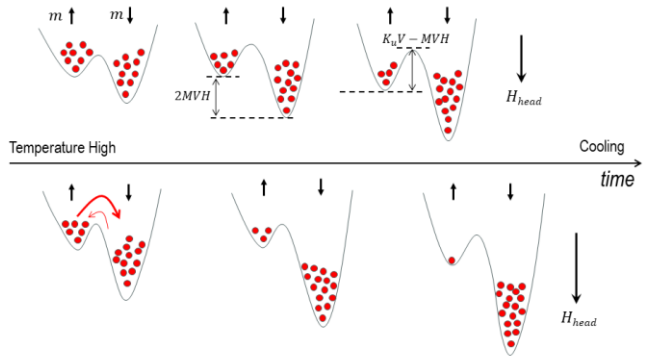

Fig. 8. Illustration of transient magnetization states for the grains within recording zone during recording. The curve representing energy versus magnetization angle as the medium cools while moving away from the NFT. The difference between the two energy minima is due to the head field and the energy barrier due to the grain magnetocrystalline anisotropy. Upper: The case with a relatively smaller head field and the limited magnetic potential energy was not strong enough such that a number of grains have their magnetization opposite to the field direction after the energy barrier becomes too high. Lower: A stronger head field leads to much reduced the number of wrongly magnetized grans due to higher magnetic potential energy as well as extended RTW.

energy is defined below [37]

$$\eta = \frac{MV_{\text{eff}}H}{k_BT} \tag{10}$$

where k_B is Boltzmann's constant, T is the recording temperature, V_{eff} is the effective grain volume, and M is the magnetization level at the recording temperature. For HAMR, the value of η is nearly one order of magnitude smaller than that for conventional perpendicular magnetic recording, assuming the same medium grain volume. The impact of thermally excited magnetization fluctuation during recording is, thus, substantially greater in HAMR. The upper row of Fig. 8 graphically illustrates this thermal impact. The red dots in the figure indicate the magnetization state of the medium grains in the recording zone. As the medium grains cool down from Curie temperature (left to right), the energy valley for the grains whose magnetization is in the head field direction grows deeper as the grain magnetization level increases. At the same time, the barrier between the two energy valleys grows higher due to the rise of grain crystalline anisotropy energy. If time is sufficient, few grains will end in the "up" state (against downward head field) since the equilibrium probability has an exponential dependence on the difference between the two energy valleys. However, the rise of energy barrier in between the two states could block the state transition if the cooling time is too faster: grains will be magnetized, or frozen, in the wrong states, causing the "incomplete" magnetization pattern recorded, as shown in the lower field amplitude cases of Fig. 5. The noise associated with this mechanism is referred to as thermal noise. In the case with a larger field amplitude, shown in the lower row of Fig. 8, the level difference of the two energy valleys is greater and the time to the "frozen" point becomes longer, leaving fewer grains wrongly magnetized, thereby lowering thermal noise.

The wrongly magnetized grains not only cause magnetization level to be lower than the saturation remanence for

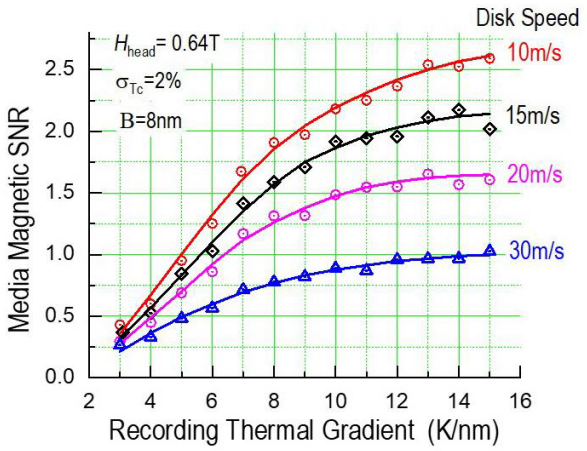

Fig. 9. Calculated recording SNR as a function of TG for a range of different disk speed during recording, all at the same exact field amplitude. Decreasing disk speed during recording significantly raises the SNR level.

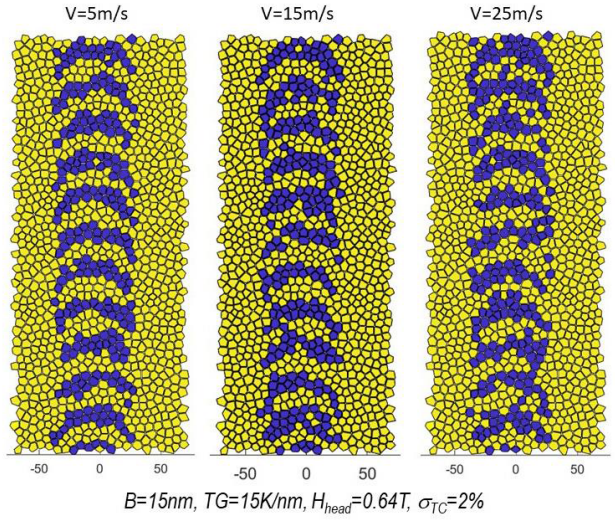

Fig. 10. Simulated recording tracks at three different disk speed over the same medium. Same head field amplitude $H_{\text{head}} = 0.64$ T is used for all recording simulations shown here. At higher speeds, the number of wrongly magnetized grains is evidently more than that at the lower recording speed.

the regions in between adjacent transitions, but also cause transition position to shift randomly, i.e., transition jitter noise, if the grains happen to be in the transitions.

In the case of insufficient head field amplitude, slowing down the recording process can help to suppress the percentage of those "wrongly" magnetized grains since the system will have more time to relax to the state with lower magnetic potential energy before the anisotropy of the grain becomes too high. Fig. 9 shows the calculated SNR as a function of recording TG for a range of disk speed at the same head field amplitude: $H_{\text{head}} = 0.64$ Tesla. The reduction of disk speed from 30 to 10 m/s yields a significant increase of SNR. With high recording TG, slowing down disk speed can significantly raise the SNR. In practice, lower head field amplitude should cause greater difference in SNR between recording at the inner diameter and the outer diameter of a disk.

Fig. 10 shows simulated recording tracks for three different writing disk speeds. The recorded magnetization pattern is

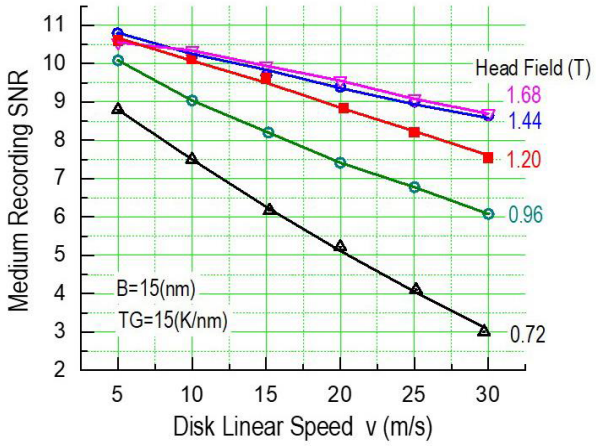

Fig. 11. Calculate recording SNR as a function of disk speed for a range of different head field amplitude in recording. The linear recording density in all the cases is the same: $D = 1.7$ MFCI. The same TG, TG = 15 K/nm is used for recording in all cases in this figure.

evidently more "regular" at the lower speeds whereas more "random" at the higher ones. Similar to the lower field amplitude cases shown in Fig. 6, the higher speed cases in this figure have more grain with their magnetization "frozen" in wrong directions while at the lower speed cases, the wrongly magnetized grains are apparently less. Since the head field amplitude in this case is relatively low, even at $v = 5$ m/s, we still can find oppositely magnetized grains in the middle of a bit region due to the recording time window (RTW) is still insufficient. In this case, further reduction of disk speed could still yield a further reduction of thermal noise.

From the above discussion, one can see that the SNR dependence on disk speed should be a function of head field amplitude. In Fig. 11, SNR as a function of disk speed is plotted for a range of head field amplitudes. Note the recording TG is fixed at TG = 15 K/nm. The speed dependence of the SNR is stronger for lower field amplitudes and is weaker for higher field amplitudes. Increasing recording field amplitude decreases the possibility for grains' magnetization to be frozen in wrong directions, thereby alleviating the need for longer RTW. However, if the field amplitude is too high, erasure-after-write starts to become significant. Reducing disk speed will further aid this degradation. In principle, if the erasure-after-write can be avoided with sufficiently high TG, thermal noise in HAMR media can completely be eliminated with sufficient long RTW and sufficient high field amplitude.

With finite recording TG, even at TG = 15 K/nm, erasure-after-write and thermal noise caused by insufficient RTW co-exist at relatively high field amplitude, as Fig. 12 illustrates. As shown in the figure, the SNR leveling off at higher field amplitudes indicates the increased presence of erasure-after-write while thermal noise still not yet vanished as the SNR can still be enhanced with decreasing disk speed. To completely eliminate thermal noise with either high head field amplitude or/and slow disk writing speed, sufficiently high TG is critical to avoid erasure-after-write.

To further illustrate the interdependence of the SNR on both the linear density and recording speed, Fig. 13 plots the calculated recording SNR contours (numbers are in dB) as

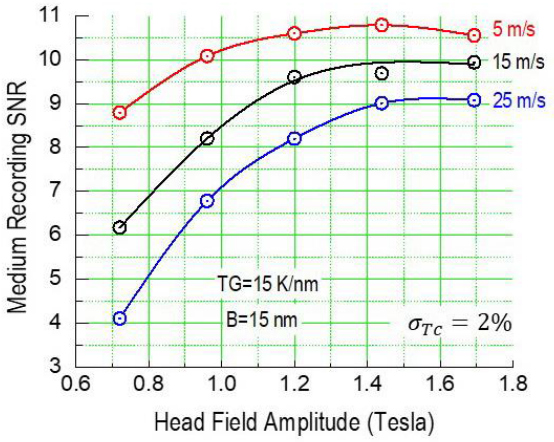

Fig. 12. Calculated recording SNR as a function of head field amplitude for three difference disk speed during writing.

a function of recording linear density and writing data rate (note no electronic noise is included here.). Three cases with different head field amplitudes, $H_{\text{head}} = 0.64$ Tesla (upper), 0.80 Tesla (middle), and 1.2 Tesla (lower) are shown here. Recording TG is fixed at TG = 15 K/nm. When the field amplitude is relatively low, lowering the write data rate enables significantly higher linear density while maintaining SNR. However, at relative high head field amplitude, the SNR gain by reducing the write data rate becomes much limited and the dependence on the write data rate is significantly less. These results are very much consistent with the ones shown in Fig. 11.

The SNR dependence on both the head field amplitude and the recording linear speed can be explained by the RTW which was first proposed in [7] with further in depth studies in [8]. Substituting recording temperature $T_{\text{Recording}}$ with head field amplitude H_{head}, one obtains the following expression:

$$\text{RTW} = \frac{(T_C - 300)}{\text{TG} \cdot v} \cdot \left(\frac{\beta H_{\text{head}}}{H_{k,\text{RT}}}\right)^{\frac{3}{1.1}} \tag{11}$$

where T_c is Curie temperature of media in Kelvin, TG is recording TG in K/nm, v is disk linear velocity (speed), $H_{k,\text{RT}}$ is anisotropy field at room temperature (300 K), and βH_{head} is the maximum anisotropy field of the grain can be switched by the head field, H_{head}, with the value of β in the between [1.0, 2.0], depending on the field angle at the location where transition is written. Insufficient value of RTW can lead to low SNR whereas prolonged RTW yields erasure-after-write [7], causing SNR to degrade. Relatively low head field amplitude combining with higher recording speed always leads to insufficient RTW. Equation (11) can be used to estimate the RTW for both modeling and spin stand measurements.

To put things in perspective, Fig. 14 shows the comparison of recording SNR as a function of recording TG for two cases: media with and without grain-to-grain Curie temperature variation. Here the recording head field amplitude is purposely chosen to be relatively high. For the case with $\sigma_{Tc} = 2\%$, (red curve in the figure) increasing TG yields a monotonic increase of SNR value as stated before. For the case without

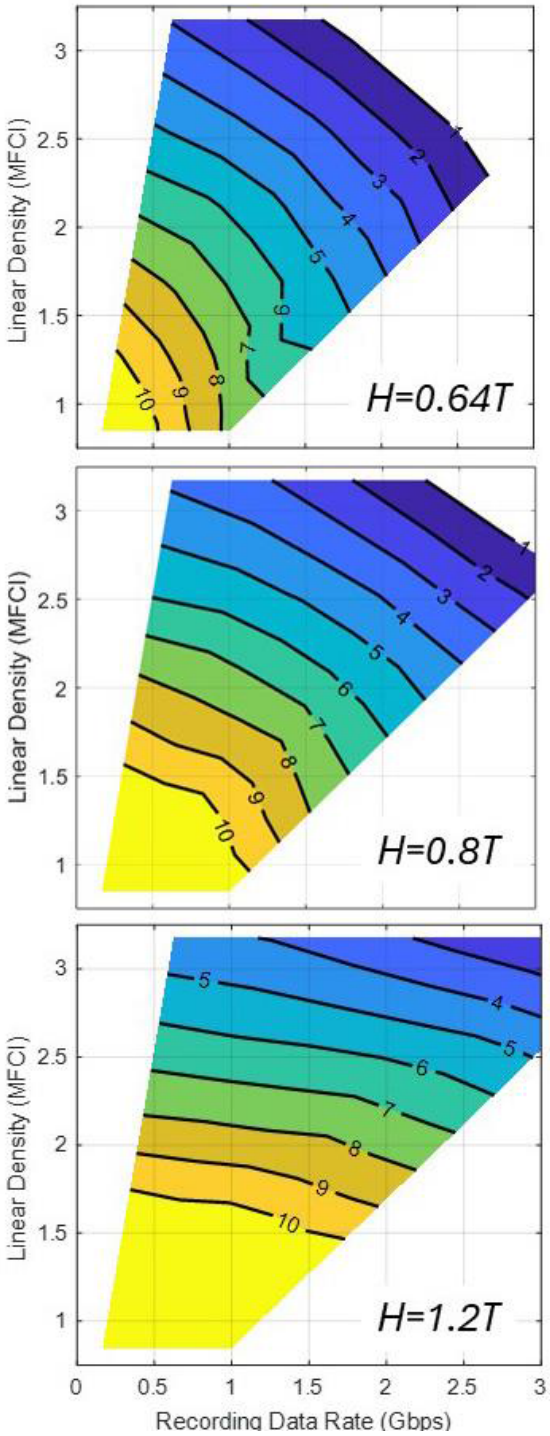

Fig. 13. Calculated recording SNR contours (in dB) as function of recording linear density and writing data rate for three different head field amplitudes. The recording thermal gradient of TG = 15 K/nm is used. A Tc distribution of $\sigma_{Tc} = 2\%$ is assumed over the grains in the medium. The SNR values are also indicated by the color mapping.

grain-to-grain Curie temperature variation, $\sigma_{Tc} = 0$ (blue curve), the recording SNR is significantly higher than that in the case $\sigma_{Tc} = 2\%$, however, the SNR shows a peak value around 9 K/nm. Below this optimal TG value, erasure-after-write is the main cause for the SNR reduction due to relatively poor TG. For TG greater than the optimum, the RTW becomes insufficiently short, and reduction of the RTW causes

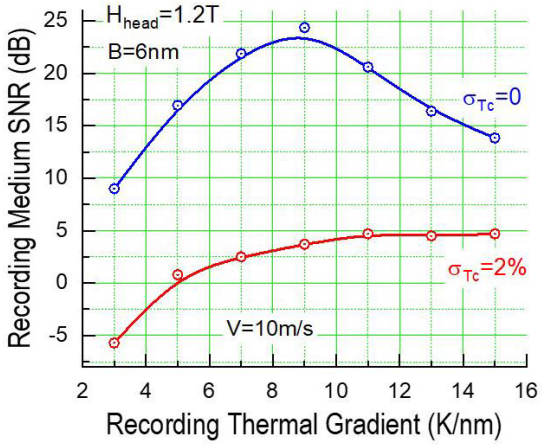

Fig. 14. Calculated recording SNR as a function of recording TG for the case of $\sigma_{Tc} = 0$ (blue) and the case of $\sigma_{Tc} = 2\%$ (red). The head field amplitude is 1.2 Tesla, the recording bit length is $B = 6$ nm and the disk linear speed is $v = 10$ m/s.

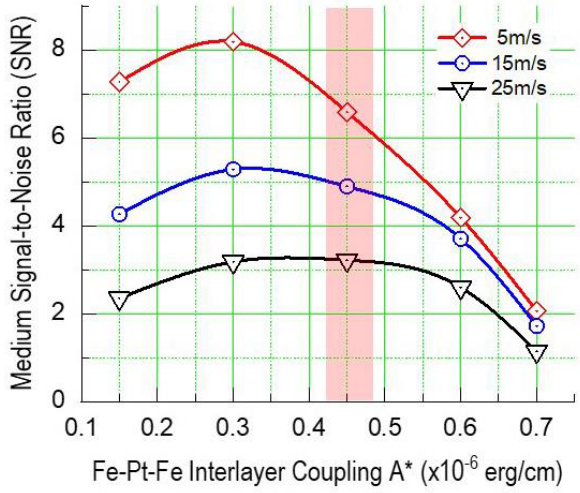

Fig. 15. Calculated recording SNR as a function of the effective Fe-Fe exchange coupling stiffness constant A^* for three cases, each at a different disk speed. The head field amplitude is set at $H_{\text{head}} = 0.64$ Tesla and the linear recording density is $D = 1.7$ MFCI.

the degradation of SNR. A higher disk speed will move the optimum TG value toward a lower value. A higher recording field amplitude would require a higher TG to avoid worsening of erasure-after-write.

Before ending this section, we would like to address the choice of the effective exchange stiffness constant, A^*, which measures the ferromagnetic exchange coupling between the adjacent Fe atomic monolayers within a $L1_0$ ordered FePt grain. Fig. 15 shows calculated recording SNR as a function of the effective exchange stiffness constant for three different recording speeds. The head field amplitude for the recording is $H_{\text{head}} = 0.64$ Tesla and the linear density for the recording simulation is $D \approx 1.7$ MFCI (bit length $B = 15$ nm). (In reference that the exchange stiffness constant for bcc Fe is $A = 1.3 \times 10^{-6}$ erg/cm.) The pink-shaded value $A_0^* = 0.45 \times 10^{-6}$ erg/cm is the value that used for all the calculations presented in article and is chosen based on comparison with experimental measurements [26]. Note that the effective exchange stiffness constant for adjacent Fe monolayers should be dependent on the $L1_0$ order parameter since any substitution with Fe atoms in a Pt monolayer should increase the exchange coupling between two adjacent Fe monolayers, hence likely to increase the value of A^*. At the chosen A_0^* value, all the macro-spins within a grain are oriented in the same direction at the end of a recording process. Even though during recording, magnetization switching could be incoherent, and it usually are, after temperature returns to ambient, every grain is essentially in a single domain state with all 30 macro-spins oriented in the same direction with no residual domain wall left within a grain stack.

IV. Conclusion and Remarks

A novel micromagnetic model developed based on the atomic structure of $L1_0$ ordered FePt grains is employed to study the HAMR in granular FePt-$L1_0$ thin film media. The study found that the medium noise arising from grain-to-grain Curie temperature variation can be completely suppressed with sufficient TG and sufficiently high head field amplitude. The broader the T_c distribution requires the higher TG and the greater field amplitude.

The other dominant noise source in HAMR is the thermal noise caused by the magnetization of the grains in the recording zone frozen to the opposition direction of the head field during recording processes. The thermal noise could dominate if the head field amplitude is insufficient and disk speed is high which leads to insufficient RTW. Raising head field amplitude or slowing down disk speed during recording could sufficiently suppress the noise and achieving grain pitch limited recording SNR as long as recording TG is sufficiently high to prevent any erasure-after-write.

The strong head field amplitude dependence of the thermal noise points at a possible cause for the broad variation of head-to-head SNR performance widely observed in practice. In HAMR, the footprint of write-head main pole is much larger than that in conventional perpendicular magnetic recording. The large dimension of the main pole gives rise to the possibility of complex domain formations during recording process which is a very plausible reason for the observed head-to-head performance variation as well as dynamic variations of the head field amplitude during recording.

Incorporating the essential physics based on the atomic structure of $L1_0$ FePt grain is evidently critical for correctly modeling the physical behavior of the granular media during recording. Since the ferromagnetic exchange coupling between the adjacent Fe monolayers (interlayer coupling) and within each Fe monolayer (intra-layer coupling) is significantly different, Curie temperature of perpendicularly ordered $L1_0$ granular FePt films should have a significantly stronger dependence on grain size than that on grain height. Specific experimental measurements for quantitatively determining the interlayer exchange coupling between adjacent Fe monolayers within a highly $L1_0$ ordered FePt grains are needed.

The relatively weak ferromagnetic exchange coupling in the ordering direction for $L1_0$ FePt grains would also imply that increasing grain height is not as effective as increasing grain

diameter in terms of having sufficient grain volume. Even greater grain height might be needed as grain diameter reduces for higher area density capabilities [37].

ACKNOWLEDGMENT

The author would like to thank Dr. Tobias Maletzky and Dr. Moris Dovek for initiating this research and elucidating discussions. This work was supported in part by the Data Storage Systems Center and its industrial sponsors, and Kavck-Moura Fund at Carnegie Mellon University.

REFERENCES

[1] M. H. Kryder et al., "Heat assisted magnetic recording," *Proc. IEEE*, vol. 96, no. 11, pp. 1810–1835, Nov. 2008, doi: 10.1109/JPROC.2008.2004315.

[2] W. A. Challener et al., "Heat-assisted magnetic recording by a near-field transducer with efficient optical energy transfer," *Nature Photon.*, vol. 3, pp. 220–224, Mar. 2009.

[3] B. C. Stipe et al., "Magnetic recording at 1.5 Pb m^{-2} using an integrated plasmonic antenna," *Nature Photon.*, vol. 4, no. 7, pp. 484–488, Jul. 2010.

[4] A. Q. Wu et al., "HAMR areal density demonstration of 1+ Tbpsi on spinstand," *IEEE Trans. Magn.*, vol. 49, no. 2, pp. 779–782, Feb. 2013, doi: 10.1109/TMAG.2012.2219513.

[5] G. Ju et al., "High density heat-assisted magnetic recording media and advanced characterization—Progress and challenges," *IEEE Trans. Magn.*, vol. 51, no. 11, pp. 1–9, Nov. 2015, doi: 10.1109/TMAG.2015.2439690.

[6] C. Rea et al., "High track pitch capability for HAMR recording," *IEEE Trans. Magn.*, vol. 53, no. 2, pp. 1–7, Feb. 2017, doi: 10.1109/TMAG.2016.2614913.

[7] J.-G. Zhu and H. Li, "Understanding signal and noise in heat assisted magnetic recording," *IEEE Trans. Magn.*, vol. 49, no. 2, pp. 765–772, Feb. 2013.

[8] R. H. Victora and P.-W. Huang, "Simulation of heat-assisted magnetic recording using renormalized media cells," *IEEE Trans. Magn.*, vol. 49, no. 2, pp. 751–757, Feb. 2013.

[9] R. F. L. Evans, W. J. Fan, P. Chureemart, T. A. Ostler, M. O. A. Ellis, and R. W. Chantrell, "Atomistic spin model simulations of magnetic nanomaterials," *J. Phys., Condens. Matter*, vol. 26, no. 10, Mar. 2014, Art. no. 103202.

[10] S. J. Greaves, H. Muraoka, and Y. Kanai, "Modelling of heat assisted magnetic recording with the Landau-Lifshitz-Bloch equation and Brillouin functions," *J. Appl. Phys.*, vol. 117, no. 17, May 2015, Art. no. 17C505.

[11] C. Vogler, C. Abert, F. Bruckner, D. Suess, and D. Praetorius, "Areal density optimizations for heat-assisted magnetic recording of high-density media," *J. Appl. Phys.*, vol. 119, no. 22, Jun. 2016, Art. no. 223903.

[12] N. A. Natekar, E. Roddick, and R. M. Brockie, "Interplay of the thermal and magnetic fields in HAMR," *IEEE Trans. Magn.*, vol. 58, no. 4, pp. 1–8, Apr. 2022.

[13] Y. Jiao, J. Hohlfield, and R. H. Victora, "Understanding transition and remanence noise in HAMR," *IEEE Trans. Magn.*, vol. 54, no. 11, pp. 1–5, Nov. 2018.

[14] H. Li and J.-G. Zhu, "Understanding the impact of T_c and H_k variation on signal-to-noise ratio in heat-assisted magnetic recording," *J. Appl. Phys.*, vol. 115, no. 17, May 2014, Art. no. 17B744.

[15] J. J. Zhu and H. Li, "Correcting transition curvature in heat-assisted magnetic recording," *IEEE Trans. Magn.*, vol. 53, no. 2, pp. 1–7, Feb. 2017, doi: 10.1109/TMAG.2016.2614836.

[16] S. Hernandez et al., "Geometrical scaling limits of heat-assisted magnetic recording," *IEEE Trans. Magn.*, vol. 57, no. 3, pp. 1–5, Mar. 2021, doi: 10.1109/TMAG.2020.3040497.

[17] E. Roddick, L. Xu, and R. M. Brockie, "Component design considerations for high areal density in heat-assisted magnetic recording," *IEEE Trans. Magn.*, vol. 57, no. 2, pp. 1–7, Feb. 2021, doi: 10.1109/TMAG.2020.3012941.

[18] A. F. Torabi, J. Van Ek, E. Champion, and J. Wang, "Micromagnetic modeling study of thermal gradient effect in heat-assisted magnetic recording (HAMR)," *IEEE Trans. Magn.*, vol. 45, no. 10, pp. 3848–3850, Oct. 2009, doi: 10.1109/TMAG.2009.2023877.

[19] N. A. Natekar, Z. Liu, S. Hernandez, and R. H. Victora, "SNR improvement by variation of recording and media parameters for a HAMR exchange coupled composite media," *AIP Adv.*, vol. 8, no. 5, May 2018, Art. no. 056513, doi: 10.1063/1.5007072.

[20] Z. Li, D. Wei, and F. Wei, "Micromagnetic modeling for heat-assisted magnetic recording," *J. Magn. Magn. Mater.*, vol. 320, no. 22, pp. 3108–3112, Nov. 2008, doi: 10.1016/j.jmmm.2008.08.085.

[21] J.-G. Zhu and Y. Yan, "Incoherent magnetic switching of L10 FePt grains," *IEEE Trans. Magn.*, vol. 57, no. 3, Mar. 2021, Art. no. 3200809.

[22] K. Xue and R. H. Victora, "Dependence of HAMR transition curvature on bit length," *IEEE Trans. Magn.*, vol. 58, no. 2, pp. 1–5, Feb. 2022, doi: 10.1109/TMAG.2021.3083716.

[23] N. A. Natekar, W. Tipcharoen, and R. H. Victora, "Composite media with reduced write temperature for heat assisted magnetic recording," *J. Magn. Magn. Mater.*, vol. 486, Sep. 2019, Art. no. 165253, doi: 10.1016/j.jmmm.2019.165253.

[24] L. Xu, R. M. Brockie, N. A. Natekar, and E. Roddick, "The scaling capability of heat assisted magnetic recording," *IEEE Trans. Magn.*, vol. 59, no. 3, pp. 1–7, Mar. 2023, doi: 10.1109/TMAG.2022.3221782.

[25] D. A. Saunders, J. Hohlfeld, X. Zheng, T. Rausch, and C. Rea, "HAMR thermal gradient measurements and analysis," *IEEE Trans. Magn.*, vol. 53, no. 2, Feb. 2017, Art. no. 3100305.

[26] T. Maletzky, A. Lai, K. Lau, B. Valcu, and M. Dovek, unpublished results, 2022.

[27] D. Weller et al., "High K_u materials approach to 100 Gbits/in^2," *IEEE Trans. Magn.*, vol. 36, no. 1, pp. 10–15, Jan. 2000, doi: 10.1109/20.824418.

[28] D. E. Laughlin, K. Srinivasan, M. Tanase, and L. Wang, "Crystallographic aspects of L10 magnetic materials," *Scripta Mater.*, vol. 53, no. 4, pp. 383–388, Aug. 2005.

[29] R. Evans, "Atomistic modeling of nanogrnular magnetic materials," Ph.D. thesis, Dept. Phys., Univ. of York, York, U.K., 2008, p. 29.

[30] H. J. Richter and G. J. Parker, "Temperature dependence of the anisotropy field of L1 FePt near the Curie temperature," *J. Appl. Phys.*, vol. 121, no. 21, Jun. 2017, Art. no. 213902, doi: 10.1063/1.4984911.

[31] N. Smith and P. Arnett, "White-noise magnetization fluctuations in magnetoresistive heads," *Appl. Phys. Lett.*, vol. 78, no. 10, pp. 1448–1450, Mar. 2001.

[32] J.-G. Zhu, "Thermal magnetic noise and spectra in spin valve heads," *J. Appl. Phys.*, vol. 91, no. 10, pp. 7273–7275, May 2002.

[33] J.-G. Zhu, "Magnietization dyanmics: Thermal-driven noise in magnetoresistive sensors," in *Handbook of Magnetism and Advanced Magnetic Materials*, vol. 2, H. Kronmuller and S. Parkin, Eds., 2007, pp. 1083–1091, doi: 10.1002/9780470022184.hmm216.

[34] T. Qu and R. H. Victora, "Effect of substitutional defects on Kambersky damping in L1 magnetic materials," *Appl. Phys. Lett.*, vol. 106, no. 7, Feb. 2015, Art. no. 072404, doi: 10.1063/1.4909510.

[35] N. A. Natekar, W.-H. Hsu, and R. H. Victora, "Calculated dependence of FePt damping on external field magnitude and direction," *AIP Adv.*, vol. 7, no. 5, May 2017, Art. no. 056004, doi: 10.1063/1.4973800.

[36] T. A. Ostler, M. O. A. Ellis, D. Hinzke, and U. Nowak, "Temperature-dependent ferromagnetic resonance via the Landau-Lifshitz-Bloch equation: Application to FePt," *Phys. Rev. B, Condens. Matter*, vol. 90, no. 9, Sep. 2014, Art. no. 094402, doi: 10.1103/PhysRevB.90.094402.

[37] Y. Qin and J.-G. Zhu, "Impact of magnetic medium grain height in heat-assisted magnetic recording," *IEEE Magn. Lett.*, vol. 10, 2019, Art. no. 6502305.